




Enhancing joint strength: investigating different interlayer effects on Ultrasonic spot-welded NiTi/304 stainless steel

Yi Chen¹ · Mingpeng Cheng¹ · Chao Liu² · Yang Li¹ · Zhen Luo¹ · Sansan Ao^{1,3} 

Received: 7 June 2023 / Accepted: 4 October 2023 / Published online: 19 October 2023
© The Author(s), under exclusive licence to Springer-Verlag London Ltd., part of Springer Nature 2023

Abstract

Ultrasonic spot welding (USW) is an emerging solid-state joining technology with great potential for solving joining challenges in Ni–Ti shape memory alloys and stainless steel (SS). In this study, USW was utilized to successfully lap weld Ni–Ti shape memory alloy and 304 SS, where copper and aluminum were introduced as separate interlayers to enhance the strength of the joint. The results show that USW can achieve effective bonding between Ni–Ti foil and 304 SS foil with or without an interlayer. In the absence of an interlayer, a mechanical interlocking structure is formed between Ni–Ti and 304 SS with a tensile strength of 404.71 N, which is lower than that of the joint with the addition of an interlayer. With the introduction of the interlayer, a double-interface structure is formed. It should be noted that the highest bond strengths were obtained with the aluminum interlayer, with a peak load of 890 N and edge fracture, although trace amounts of the brittle intermetallic compound $\text{Fe}_3\text{Al}_{14}$ were generated. A slightly lower joint strength of 690 N was obtained with the copper interlayer, but the formation of brittle intermetallic compounds was effectively avoided. These results have important implications for the successful bonding of NiTi with dissimilar materials.

Keywords Ultrasonic spot welding · NiTi shape memory alloys · 304SS · Microstructure · Mechanical properties

1 Introduction

In recent decades, shape memory alloys (SMAs) have garnered significant attention due to their distinctive shape memory effect (SME) and exceptional super-elasticity (SE). They have found applications in various fields, including aerospace,

the automotive industry, petroleum mining, microelectronics, and biomedicine [1]. NiTi alloys exhibit excellent biocompatibility and corrosion resistance in addition to the advantages mentioned above [2]. Even so, the utilization of NiTi alloy remains restricted due to its high cost, limited processability, and vulnerability to potential damage to its shape memory effect (SME) and super-elasticity (SE) properties [3–5]. It is very important to actively develop the connection between NiTi alloy and other dissimilar materials. Stainless steel (SS) has long been used in the biomedical field as a common structural material, with high biocompatibility, corrosion resistance, good mechanical properties, and various other advantages.

Highlights

- USW creates NiTi/304SS joints with varied interlayers, impacting microstructure and mechanical properties.
- Double interface characteristics achieved in USW using different interlayers.
- Improved joint strength observed with addition of Al foil interlayer in NiTi/304SS USW.

✉ Chao Liu
charlouisdas@zju.edu.cn

✉ Sansan Ao
ao33@tju.edu.cn

Yi Chen
cyttbest@163.com

Mingpeng Cheng
2019208169@tju.edu.cn

Yang Li
liyang86@tju.edu.cn

Zhen Luo
lz_tju@163.com

¹ School of Materials Science and Engineering, Tianjin University, No. 135 Yaguan Road, Haihe Education Park, Tianjin 300072, China

² College of Education, Zhejiang University, Hangzhou 310058, Zhejiang, China

³ China Engineering Construction Welding Association, Beijing 100082, China

Simultaneously, it offers affordability and convenient access to raw materials [6]. Thus, achieving effective connections between NiTi alloys and SS will further expand their range of application. Ultimately, the entire connect system will benefit from the inherent properties of the two materials.

Researches have been carried out on the reliable connection between NiTi alloys and SS, the connection methods are categorized into three aspects: fusion welding, solid phase welding, and brazing. Shamsolhodaie et al. used laser offset welding to join NiTi/SS (400 μm). By precisely directing the laser beam from the NiTi substrate to the stainless steel substrate, the formation of intermetallic compounds is effectively minimized, subsequently enhancing the properties of the joint [7]. Niu et al. used vacuum electron beam welding to join NiTi and SS plates; all of the joints (no interlayer, pure Ni, and FeNi interlayer) fractured in the weld zone close to the NiTi side due to the enrichment of the intermetallic compounds Fe_2Ti and Ni_3Ti [8]. Fukumoto et al. joined NiTi alloy and austenitic stainless steel rods with a diameter of 2.5 mm by rotary friction welding, and they found that when the Ni interlayer was used, the Fe_2Ti intermediate phase in the weld was suppressed, the interface consisted of NiTi + Ni₃Ti eutectic reaction layer, and the tensile strength of the joint increased to 510 MPa [9]. In Zhang et al., high-strength NiTi-SS wire joints were realized by laser brazing butt welding, where the beam was deflected from 0.4 mm on the NiTi side to 0.4 mm on the SS side, and the tensile strength was increased to 329.5 MPa, while the welded joints with different deflections exhibited different fracture forms [10]. Bagheri et al. have also conducted many studies on friction stir welding and friction stir brazing [11–18].

For these processes, there are some problems: (1) due to the large difference in the coefficient of linear expansion of the two base materials, there is a large welding stress in the joint; (2) the heat input is large which will also generate a large number of brittle intermetallic compounds in the weld, and at the same time there is a large inhomogeneity in the chemical composition and organization of the weld.

Ultrasonic spot welding (USW) is a solid-state welding technique. It involves applying clamping and shear forces to the welding head to induce relative movement between the metal components. This movement results in the plastic deformation of the metals, ultimately leading to their connection. This is a new way to connect NiTi alloys with SS. At present, ultrasonic welding research mainly focus on light metals (Al, Cu, Mg, etc.) connections due

to the limited input energy. Research on cemented carbide and dissimilar materials mainly centers around the welding process, microstructure, properties and the connection mechanism analysis, and so on. Satpathy et al. used the USW time mode to weld AA3003 aluminum alloy to 304 stainless steel with a copper interlayer, and found that a stronger joint was obtained when the aluminum alloy on the top [19]. Zhang et al. realized the ultrasonic spot welding of 0.2-mm-thick of NiTi alloy, and studied the bonding mechanism and joints properties [20]. Based on the study of Chunjie Li et al. further explored the influence of the Al interlayer on the mechanical properties and microstructure of 0.5-mm-thick NiTi alloy ultrasonic joint [21–23].

Realizing a good connection between NiTi and SS is of great significance in the fields of biomedicine as well as robotic chips, such as guide wire for catheters. In this paper, ultrasonic spot welding was used to join NiTi and SS to investigate the microstructure and mechanical properties of the joints for each of the three interlayer cases. This will eliminate the problems associated with conventional welding and effectively overcome the limitations of large amounts of intermetallic compounds and coarse grains in the joint. Provides options for different service conditions.

2 Materials and method

The base materials were NiTi alloy and 304SS, with 0.15-mm thickness. Cut the specimen into a welded specimen of 60 mm \times 15 mm by EDM, remove the oxide film on the surface of NiTi alloy and stainless steel with 400 # sandpaper, then clean it with alcohol and blow it dry. It should be noted that the NiTi alloy is a completely austenitic phase at room temperature. Additionally, 0.02-mm-thick Cu or Al were employed as interlayers. The chemical composition and mechanical properties of the base materials are presented in Tables 1 and 2, respectively.

We used a SONICS MSC4000-20 ultrasonic welding system equipped with a rated maximum power of 4 kW, a resonant frequency of 20 kHz, a tip amplitude range of 14 to 72 μm , and a maximum pressure of 65 psi. Figure 1 shows the lap diagram and the size of the samples. The welded specimen is cut by EDM to obtain a welded cross section, sanded with 400# to 3000# sandpaper, and then polished for

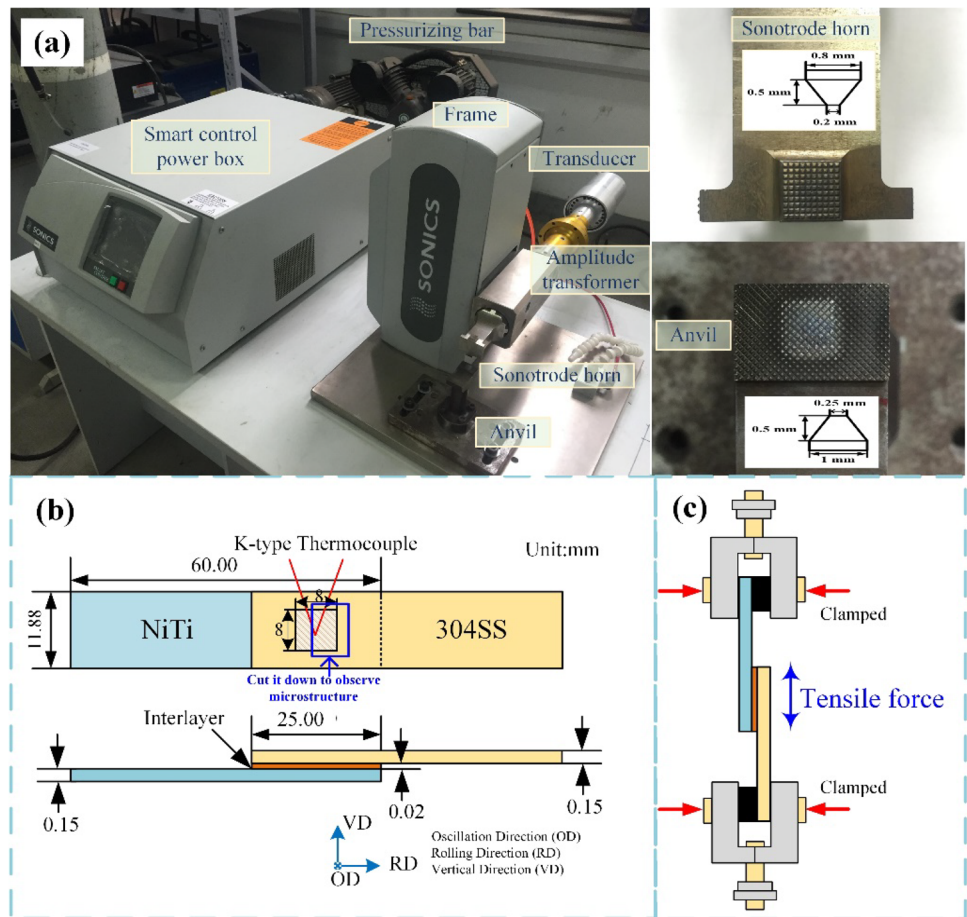
Table 1 Chemical composition of NiTi alloy and 304SS

Material	Ni	Ti	Cr	Mn	Si	Fe
NiTi	55.87	44.13	-	-	-	-
304SS	9.40	-	18.40	1.40	0.63	Bal

Table 2 Mechanical properties of NiTi alloy and 304SS

Material	Yield strength (MPa)	Tensile strength (MPa)	Hardness (HV _{0.2})	Coefficient of linear expansion (10 ⁻⁶ °C ⁻¹)	Melt point (°C)	Young modulus (GPa)
NiTi	467	639	245	10	1310	41
304SS	269	705	190	17	1440	193

Fig. 1 a Ultrasonic spot weld equipment. b Schematic diagram of lap joint. c Schematic diagram of tensile test



observation of microstructure and elemental distribution. The welded specimen as a whole will be subjected to shear tensile testing; the tensile test follows ASTM D1002.

The optimum parameters and the lap method were obtained by an extensive orthogonal experiment; the specific parameters are shown in Table 3.

Table 3 parameters and lap type of different interlayer

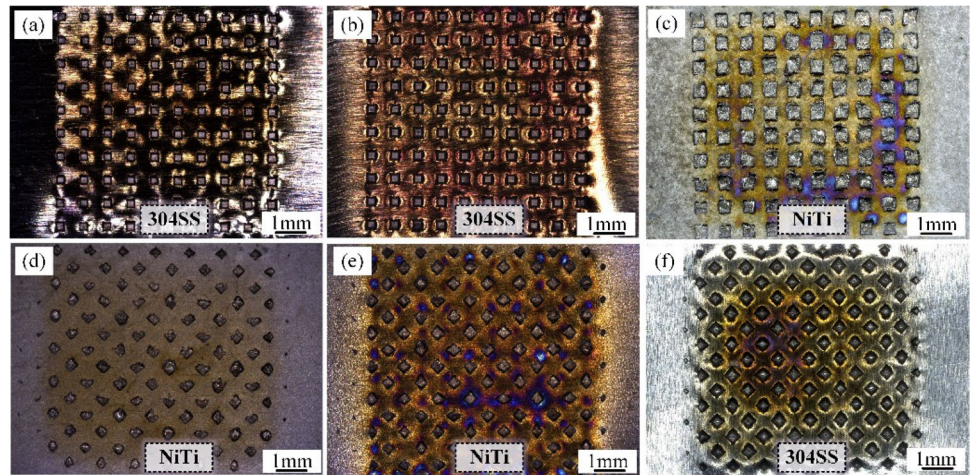
Material	Energy	Pressure	Amplitude	Lap type
No interlayer	750 J	58 psi	65 μm	304SS-NiTi
Al interlayer	750 J	51 psi	60 μm	304SS-NiTi
Cu interlayer	750 J	58 psi	55 μm	NiTi-304SS

3 Results and discussion

3.1 Microstructure

Three different interlayer exhibit different degrees of oxidation (Fig. 2), it is worth noting that the material located at the top are more oxidized than the bottom, which is related to the movement characteristics of ultrasonic metal spot welding. During the ultrasonic welding process, the weld tip applies a normal force to clamp the material, and later a shear force-driven material friction. However, due to limitations such as the hardness of base materials, it is difficult for the sharp teeth to quickly embed in the material to drive interfacial friction, so a large amount of

Fig. 2 Macroscopic morphology of the weld surface with the addition of different interlayers. **a, d** no interlayer, **b, e** Al interlayer, **c, f** Cu interlayer



heat is generated on the material surface. And the style is exposed to air and oxidation will occur quickly when heated.

There were a few gaps and debris in the interface of the joint without interlayer, shown in Fig. 3a, which will affect the performance of the joint. Mechanical interlocking exists at the interface; the base metals had obvious plastic deformation under the action of ultrasonic vibration, shown in Fig. 3b. Bakavos et al. studied that a large number of mechanical interlocking interfaces can withstand large loads during axial tensile process, thus improving joint performance [24].

For the sample with interlayer, it is considered that interfaces exist regularly at different positions. At the bottom of the welding teeth, the interlayer is destroyed and only NiTi-SS interface exists. Around the welding teeth, the NiTi-Al/Cu-SS interface exists. Thus, the interfaces of the bottom and periphery of welding teeth were analyzed respectively.

The microstructure of the interface with Al interlayer is shown in Fig. 4. The upper and lower substrates are curled, and there is no obvious peeling at the interface as

opposed to no interlayer joints in Fig. 4a. The transition of elements at the NiTi-SS interface is steep due to the aluminum foil fails to participate in the diffusion process after being squeezed out by the tip teeth of the welding head. The microstructure around the welding teeth with Al interlayer is shown in Fig. 4b. It can be seen obviously element diffusion occurs in the SS-Al and Al-NiTi interface, there is island-like intermetallic compound formations. With high strain rate plastic deformation leads to significantly enhanced vacancy and dislocation density during the process of ultrasonic welding, which drives diffusion on both sides of the interface. EDS point scans were performed on points P1 and P2, and based on the results (Table 4) can determine that the compound is $\text{Fe}_4\text{Al}_{13}$, which is a brittle compound, too much content will affect the performance of the joint. Since the plastic deformation of the aluminum interlayer is achieved by lattice slip during tensile testing. However, the brittle phase $\text{Fe}_4\text{Al}_{13}$ hinders dislocation slip, resulting in stress concentration at the interface between the $\text{Fe}_4\text{Al}_{13}$ phase and Al, making the deformation of them incompatible. As the deformation

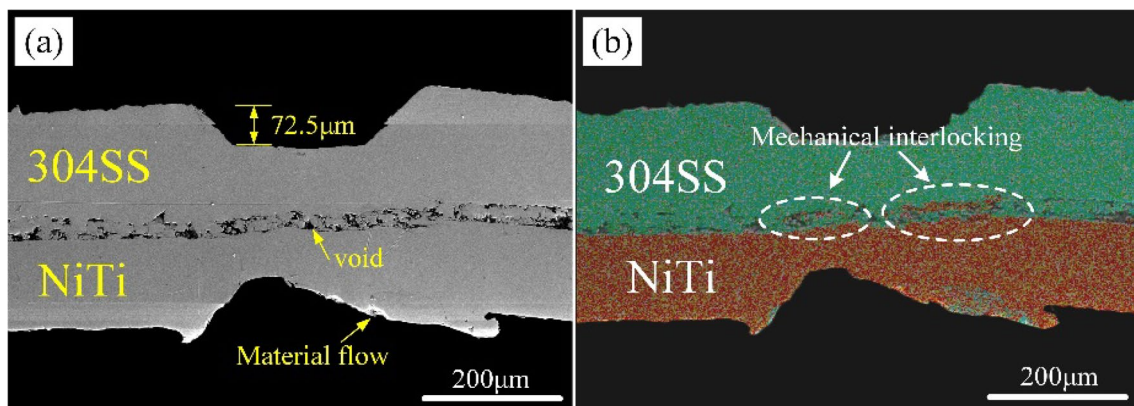


Fig. 3 **a** Interface of the joint without interlayer. **b** Mapping of **a**

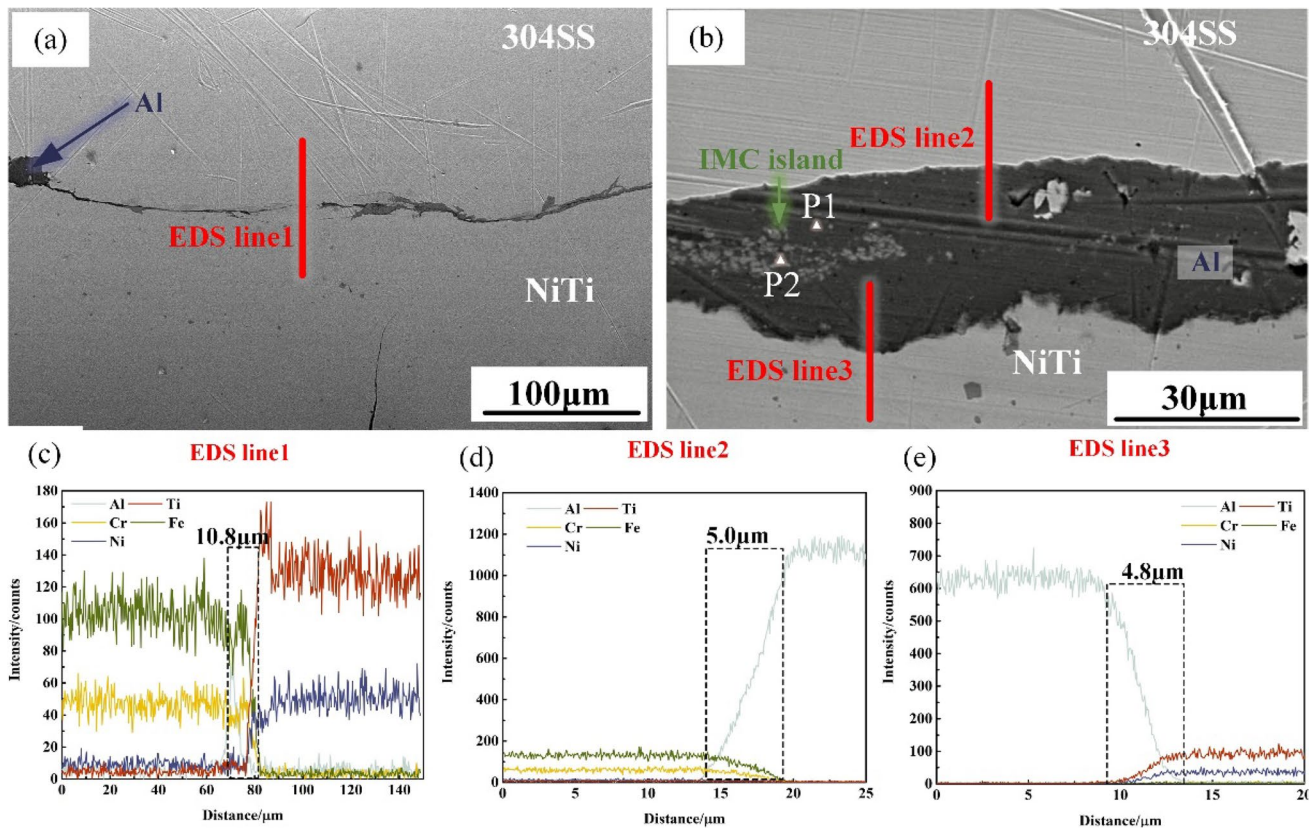


Fig. 4 **a** The microstructure of the bottom of the welding teeth with the aluminum interlayer. **b** The microstructure around the welding teeth with the aluminum interlayer. **c–e** The EDS results of the lines in **a** and **b**

Table 4 The EDS results of point P1 and P2

Elements/ position	Al	Ti	Cr	Fe	Ni
P1	99.38	0.25	0.18	0.04	0.15
P2	90.31	0.64	0.39	3.75	4.91

proceeds, the stress concentration and incompatible deformation continue to accumulate, and when accumulated to a certain extent, microcracks are generated around the Fe_4Al_{13} phase and grow. As the cracks continue to grow, fracture eventually occurs.

Diffusion distance draws our attention, the distance at the SS-Al interface is slightly larger than that at the Al-NiTi interface. The welding head drive the relative movement of 304SS and Al foil, resulting in the softening of the Al foil into a molten state and bonding with NiTi alloy. Thus, the movements of the NiTi alloy takes place behind the 304SS. However, the NiTi alloy faces challenges in undergoing plastic deformation due to its hardness. Therefore, the diffusion rate of aluminum atoms into SS is significantly higher than that of NiTi alloy, and finally leads to the difference in diffusion layer thickness [25].

Figure 5 shows the microstructure of sample with Cu interlayer, and a small number of voids appeared on the weld interface (Fig. 5a), but the proportion in the total length of the weld was small, which meant that they had no obvious adverse effect on the joint performance. These defects are usually generated in the inclined part of the crimped interface. Due to the horizontal direction of ultrasonic vibration, it is difficult to produce effective compressive stress on the inclined interface and finally exists in the interface at the end of welding [24].

The thickness of the copper that exists in the interface is different (Fig. 5b). Voids were found in the NiTi-SS interface due to the short ultrasonic welding time resulting in the failure of the copper to fill the voids after the welding was completed.

In Fig. 5c, the atomic diffusion layer of the NiTi-SS interface is very narrow, which is related to the insufficient atomic diffusion between NiTi and SS. Zhang et al. pointed out that in the process of hot isostatic pressure diffusion welding, the effective diffusion distance of Cu atoms in NiTi alloy and SS is greater than 5 μm [26]. The thermal cycle duration of ultrasonic welding is significantly shorter compared with the hot isostatic pressing process, and the peak temperature is

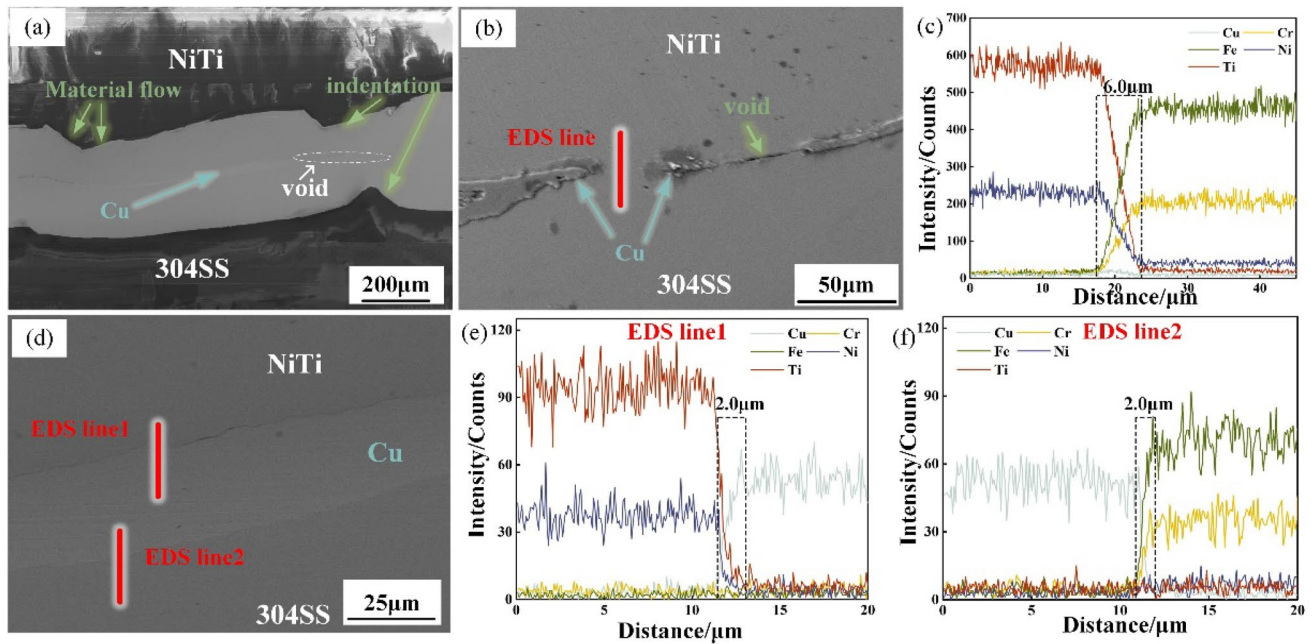


Fig. 5 **a** The microstructure of the sample with the copper interlayer. **b** The microstructure of two interface (304SS-NiTi, 304SS-Cu-NiTi) with the copper interlayer. **c** The EDS result of **b**. **d** High-magnification interface microstructure. **e**, **f** The EDS results of the lines in **d**

lower, and the lasting time at high temperatures is shorter. As a result, the diffusion of atoms over long distances will be difficult to achieve.

Figure 5 d shows the typical interface of NiTi-Cu-SS. The interfaces are closely bonded without obvious gaps. The element diffusion on both sides of the interface is very steep, and no new reaction phase is found in the micrometer scale between NiTi-Cu and Cu-SS interface. It is worth noting that the atomic diffusion distance of NiTi-SS interface is slightly longer than that of NiTi-Cu-SS interface in the specimen including the Cu interlayer. The phenomenon may be due to the larger contact stress below the tip of the welding head, and thus more plastic deformation occurs in this area, and the higher temperature promotes the atomic diffusion between NiTi alloy, Cu and SS, forming a thicker atomic diffusion layer.

From the above results, it can be seen that the diffusion distance of Al is larger than that of Cu, and island intermetallic compounds are generated in Al interlayer, indicating that the diffusion of Al is more sufficient, and it is speculated that Al is better combined with the base metal, which will be verified in the following.

3.2 Mechanical properties

The tensile test results show that only the joints with Al interlayer presented edge fracture, while the remaining two joints are interface fracture (Fig. 6), which indicates that the joints with the Al interlayer were solidly welded and the

joint strength is higher than that of the base material. In the interface fracture mode, the weld spot area is very visible, which is directly related to the tensile performance of the joint. Figure 6 d shows the peak load, the smallest value (404.71 N) occurs in specimens without interlayer while the largest (890 N) occurs in specimens with an Al interlayer.

The microstructure of no interlayer fracture shows in Fig. 7, there are scratches present near the weld spots and cracks at the edge of the weld spots. In the results of the mapping scan, it is clear that there is a bond between the two materials. As the deformation of the base metal below the tip teeth is inconsistent with that around the welding teeth during the welding process, a stress concentration will be generated at the edge of the welding spot area, and then cracks are appearing under the action of cyclic alternating load and temperature, thus becoming the weak position of the joint.

The XRD results of fracture are shown in the Fig. 7e. At room temperature, the NiTi exhibits complete (B2) austenite phase, and the 304SS exhibits complete γ -austenite phase, both of them have certain preferred orientations. The phase structure of welded NiTi is the same as that of the base metal, and no brittle phase is generated. However, after welding, the phase composition in the 304 SS is different from the base material. There are α' -(110) diffraction peak exists, indicating that stress-induced martensite transformation occurs in SS, and resulting in martensite.

The microstructures of Cu interlayer fracture are shown in Fig. 8. The fracture consists of two zones: the welding

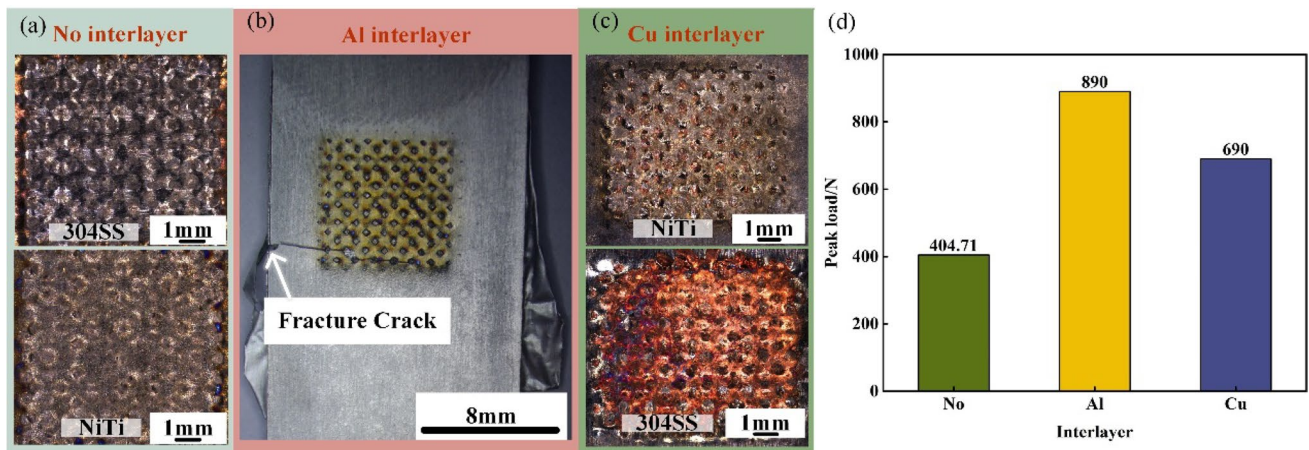


Fig. 6 Macroscopic fractures and peak load of the joints with different interlayers

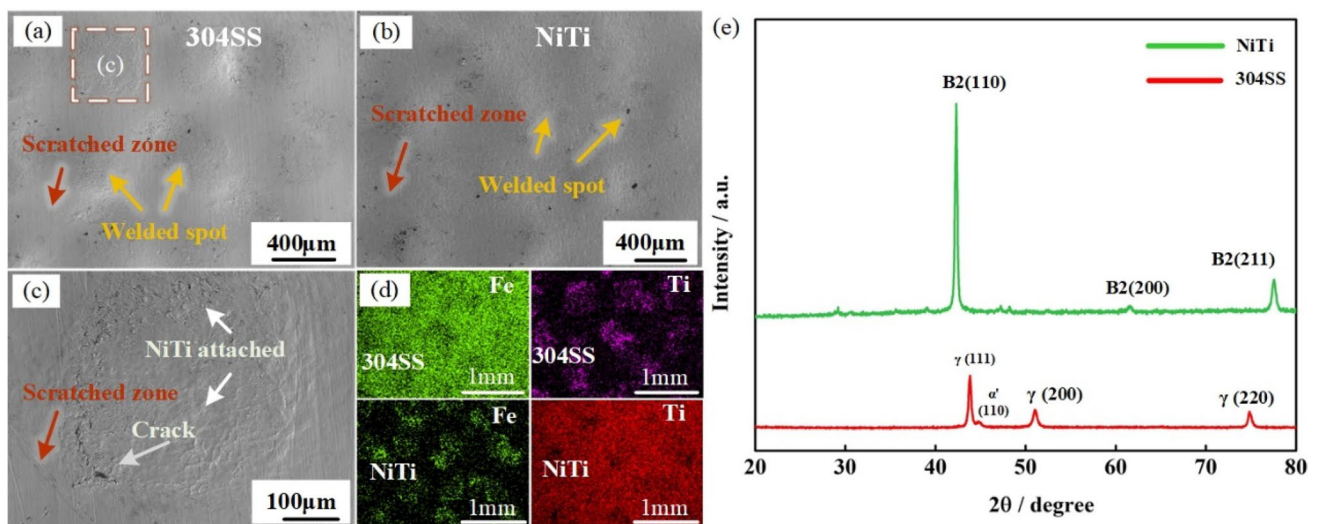


Fig. 7 The microstructure and the XRD results of fracture without interlayer

spot zone and the scratch zone. Due to the high stress concentration at the edge of the welding point during ultrasonic welding, the copper interlayer is broken below the tip teeth, and obvious cracks can be observed in the center and edge of the welding spot, indicating that the material under the tip teeth has undergone evident deformation. In Fig. 8c, a typical layered structure with a river shape and a ladder shape can be observed, indicating a brittle fracture mode at the welding spot on the NiTi alloy side. It can be seen that from EDS line scanning results (Fig. 8d), only part of the SS matrix and Cu interlayer adhered to the NiTi side under the action of ultrasonic welding. As the connection mainly occurs in the welding spot area, and the high-frequency alternating load will produce fatigue

cracks at the same time of the connection, lead to the scraping area and the edge of the welding joint area will be the weak connection areas.

XRD results are shown in Fig. 8e: a large amount of B2 austenite were found on the surface of the NiTi side while the Cu peak is less, which is consistent with the SEM analysis results (Fig. 8d). The surface of the SS fracture only contains γ -Fe phase and Cu phase, and no NiTi alloy is found. It is worth noting that the diffraction peaks of the γ -Fe and Cu phases completely overlap due to the fact that the two phases have the same crystal structure and similar lattice constants [27]. No mesophase formation was detected on the two fracture surfaces, which was consistent with EDS analysis results.

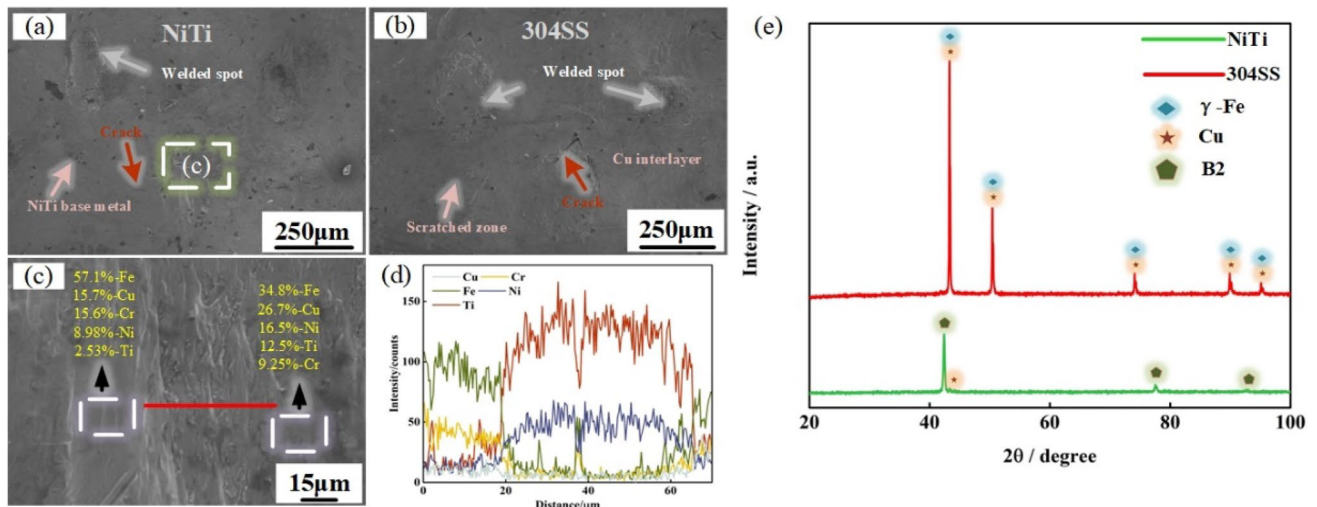


Fig. 8 The microstructure and the XRD results of fracture with Cu interlayer

4 Conclusions

We compared the microstructure and mechanical properties of NiTi and SS304 in three interlayer cases when ultrasonic welding was performed.

1. In this paper, the good connections of 304SS-NiTi, 304SS-Cu-NiTi, and NiTi-Al-304SS are realized. The joint without interlayer has a mechanical interlock structure, and the addition of copper/aluminum intermediate layer has a “double interface” structure.
2. Among the three kinds of joints, the joint with aluminum interlayer has the highest strength and the peak load is 890 N, the joint with copper interlayer has the peak load is 690 N, and the joint without interlayer has the peak load is 404.71 N.
3. The joint without the interlayer has a mechanical interlock structure. A trace amount of Fe_4Al_{13} intermetallic brittle compound appears in the joint with aluminum interlayer, which is harmful to the joint performance. No brittle compounds appear in the joint with copper interlayer, but the element diffusion distance is smaller than that with aluminum interlayer.

Author contribution Yi Chen did all the experiments and wrote this draft. Mingpeng Cheng assisted in the experiment and revised the paper. Chao Liu participated in the discussion of this whole work. Yang Li participated in the discussion of this whole work, including the instruction of the experiment. Zhen Luo participated in the discussion of this whole work, including revised the paper. Sansan Ao participated in the discussion of this whole work, including the design of the experiment.

Funding This work was supported by the National Natural Science Foundation of China (No. U1933129) and the Natural Science Foundation of Tianjin Science and Technology Correspondent Project (No. 18JQCQNJC04100, No. 19JCZDJC39000, and No. 19YFFCYS00090).

Declarations

Conflict of interest The authors declare no competing interests.

References

1. Jani JM, Leary M, Subic A, Gibson MA (2014) A review of shape memory alloy research, applications and opportunities[J]. *Mater Des* 56:1078–1113. <https://doi.org/10.1016/j.matdes.2013.11.084>
2. Guo Y, Klink A, Chenhao Fu, Snyder J (2013) Machinability and surface integrity of Nitinol shape memory alloy[J]. *CIRP Ann* 62(1):83–86. <https://doi.org/10.1016/j.cirp.2013.03.004>
3. Oliveira JP, Miranda RM, BrazFernandes FM (2017) Welding and joining of NiTi shape memory alloys: a review[J]. *Prog Mater Sci* 88:412–466. <https://doi.org/10.1016/j.pmatsci.2017.04.008>
4. Weinert K, Petzoldt V (2008) Machining NiTi micro-parts by micro-milling[J]. *Mater Sci Eng A* 481:672–675. <https://doi.org/10.1016/j.msea.2006.10.220>
5. Weinert K, Petzoldt V (2004) Machining of NiTi based shape memory alloys[J]. *Mater Sci Eng A* 378(1–2):180–184. <https://doi.org/10.1016/j.msea.2003.10.344>
6. Patnaik L, Maity SR, Kumar S (2020) Status of nickel free stainless steel in biomedical field: a review of last 10 years and what else can be done[J]. *Mater Today Proc* 26:638–643. <https://doi.org/10.1016/j.matpr.2019.12.205>
7. Shamsolhodaei A, Oliveira JP, Schell N, Maawad E, Panton B, Zhou YN (2020) Controlling intermetallic compounds formation during laser welding of NiTi to 316L stainless steel[J]. *Intermetallics* 116:106656. <https://doi.org/10.1016/j.intermet.2019.106656>
8. Niu H, Jiang HC, Zhao MJ, Rong LJ (2021) Effect of interlayer addition on microstructure and mechanical properties of NiTi/stainless steel joint by electron beam welding[J]. *J Mater Sci Technol* 61:16–24. <https://doi.org/10.1016/j.jmst.2020.05.043>
9. Fukumoto S, Inoue T, Mizuno S, Okita K, Tomita T, Yamamoto A (2010) Friction welding of TiNi alloy to stainless steel using Ni

- interlayer[J]. *Sci Technol Weld Join* 15(2):124–130. <https://doi.org/10.1179/136217109X12577814486692>
10. Zhang K, Peng P, Zhou YN (2022) Laser welding-brazing of NiTi/304 stainless steel wires with beam defocus and large offset [J]. *Mater Sci Eng A* 835 142660:0921–5093. <https://doi.org/10.1016/j.msea.2022.142660>
 11. Vaneghi AH, Bagheri B, Shamsipur A, Mirsalehi SE, Abdollahzadeh A (2022) Investigations into the formation of intermetallic compounds during pinless friction stir spot welding of AA2024-Zn-pure copper dissimilar joints[J]. *Weld World* 66:2351–2369. <https://doi.org/10.1007/s40194-022-01366-6>
 12. Abdollahzadeh A, Bagheri B, Vaneghi AH, Shamsipur A, Mirsalehi SE (2023) Advances in simulation and experimental study on intermetallic formation and thermomechanical evolution of Al–Cu composite with Zn interlayer: effect of spot pass and shoulder diameter during the pinless friction stir spot welding process [J]. *Proc Inst Mech Eng Part L J Mater Des Appl* 237(6):1475–1494. <https://doi.org/10.1177/14644207221146981>
 13. Abbasi M, Bagheri B, Sharifi F, Abdollahzadeh A (2021) Friction stir vibration brazing (FSVB): an improved version of friction stir brazing[J]. *Weld World* 65:2207–2220. <https://doi.org/10.1007/s40194-021-01173-5>
 14. Abbasi M, Baghei B (2021) New attempt to improve friction stir brazing[J]. *Mater Lett* 304 130688:0167–577X. <https://doi.org/10.1016/j.matlet.2021.130688>
 15. Rizi VS, Abbasi M, Bagheri B (2021) Investigation into microstructure and mechanical behaviors of joints made by friction stir vibration brazing between low carbon steels [J]. *Physic Script* 96:125704. <https://doi.org/10.1088/1402-4896/ac1dcb>
 16. Bagheri B, Abbasi M, Sharifi F, Abdollahzadeh A (2022) Different attempt to improve friction stir brazing: effect of mechanical vibration and rotational speed[J]. *Met Mater* 28:2239–2251. <https://doi.org/10.1007/s12540-021-01121-4>
 17. Bagheri B, Abbasi M, Sharifi F, Abdollahzadeh A (n.d) Investigation into novel multipass friction stir vibration brazing of carbon steels[J]. *Mater Manuf Process* 37:8, 921–932. <https://doi.org/10.1080/10426914.2021.2006220>
 18. Bagheri B, Alizadeh M, Mirsalehi SE, Shamsipur A, Abdollahzadeh A (2022) The effect of rotational speed and dwell time on Al/SiC/Cu composite made by friction stir spot welding[J]. *Weld World* 66:2333–2350. <https://doi.org/10.1007/s40194-022-01376-4>
 19. Satpathy MP, Patel B, Sahoo SK (2019) Exploration of bonding phenomenon and microstructural characterization during high-power ultrasonic spot welding of aluminum to steel sheets with copper interlayer[J]. *Ain Shams Eng J* 10(4):811–819. <https://doi.org/10.1016/j.asej.2019.07.007>
 20. Zhang W, Ao SS, Oliveira JP, Zeng Z, Luo Z, Hao ZZ (2018) Effect of ultrasonic spot welding on the mechanical behaviour of NiTi shape memory alloys[J]. *Smart Mater Struct* 27(8):1–6. <https://doi.org/10.1088/1361-665X/aada8f>
 21. Li C, Ao S, Oliveira JP, Cheng M, Zeng Z, Cui H, Luo Z (2020) Ultrasonic spot welded NiTi joints using an aluminum interlayer: microstructure and mechanical behavior[J]. *J Manuf Process* 56:1201–1210. <https://doi.org/10.1016/j.jmapro.2020.05.043>
 22. Li C, Ao S, Oliveira JP, Zeng Z, Cui H, Luo Z (2020) Effects of postweld heat treatment on the phase transformation and mechanical behavior of NiTi ultrasonic spot welded joints with Al interlayer[J]. *J Manuf Sci Eng* 142(10):101006. <https://doi.org/10.1115/1.4048002>
 23. Ao S, Li C, Zhang W, Oliveira JP, Zeng Z, Luo Z (2022) Effect of laser surfacing on the microstructure and mechanical properties of ultrasonic welded NiTi joints[J]. *J Manuf Sci Eng* 144(1):011003. <https://doi.org/10.1115/1.4051330>
 24. Bakavos D, Prangnell PB (2010) Mechanisms of joint and microstructure formation in high power ultrasonic spot welding 6111 aluminium automotive sheet[J]. *Mater Sci Eng A* 527(23):6320–6334. <https://doi.org/10.1016/j.msea.2010.06.038>
 25. Fujii HT, Goto Y, Sato YS, Kokawa H (2016) Microstructure and lap shear strength of the weld interface in ultrasonic welding of Al alloy to stainless steel[J]. *Scripta Mater* 116:135–138. <https://doi.org/10.1016/j.scriptamat.2016.02.004>
 26. Zhang J, Xie D, Li Q, Jiang C, Li Q (2020) Effect of holding time on the microstructure and strength of tungsten/steel joints by HIP diffusion bonded using a Cu interlayer[J]. *Mater Lett* 261:126875. <https://doi.org/10.1016/j.matlet.2019.126875>
 27. Tey CF, Tan X, Sing SL, Yeong WY (2020) Additive manufacturing of multiple materials by selective laser melting: Ti-alloy to stainless steel via a Cu-alloy interlayer[J]. *Addit Manuf* 31:100970. <https://doi.org/10.1016/j.addma.2019.100970>

Publisher's Note Springer Nature remains neutral with regard to jurisdictional claims in published maps and institutional affiliations.

Springer Nature or its licensor (e.g. a society or other partner) holds exclusive rights to this article under a publishing agreement with the author(s) or other rightsholder(s); author self-archiving of the accepted manuscript version of this article is solely governed by the terms of such publishing agreement and applicable law.